











A single evolutionarily divergent mutation determines the different FAD-binding affinities of human and rat NQO1 due to site-specific phosphorylation

Juan Luis Pacheco-García¹ , Dmitry Loginov² , Bruno Rizzuti^{3,4} , Pavla Vankova^{5,6} , Jose L. Neira^{4,7} , Daniel Kavan² , Noel Mesa-Torres¹ , Rita Guzzi^{3,8} , Petr Man²  and Angel L. Pey⁹ 

- 1 Departamento de Química Física, Facultad de Ciencias, Universidad de Granada, Spain
- 2 Institute of Microbiology of the Czech Academy of Sciences, BioCeV, Praha, Czech Republic
- 3 CNR-NANOTEC, SS Rende (CS), Department of Physics, University of Calabria, Rende, Italy
- 4 Instituto de Biocomputación y Física de los Sistemas Complejos (BIFI), Zaragoza, Spain
- 5 Institute of Biotechnology of the Czech Academy of Sciences, BioCeV, Vestec, Czech Republic
- 6 Department of Biochemistry, Faculty of Science, Charles University, Prague, Czech Republic
- 7 Instituto de Biología Molecular y Celular, Universidad Miguel Hernández, Elche, Spain
- 8 Molecular Biophysics Laboratory, Department of Physics, University of Calabria, Rende, Italy
- 9 Departamento de Química Física, Unidad de Excelencia de Química aplicada a Biomedicina y Medioambiente e Instituto de Biotecnología, Facultad de Ciencias, Universidad de Granada, Spain

Correspondence

A. L. Pey, Departamento de Química Física, Unidad de Excelencia de Química aplicada a Biomedicina y Medioambiente e Instituto de Biotecnología, Facultad de Ciencias, Universidad de Granada, Granada 18071, Spain
 Tel: +34-686469276
 E-mail: angelp@ugr.es

(Received 13 September 2021, revised 10 November 2021, accepted 10 November 2021)

doi:10.1002/1873-3468.14238

Edited by Peter Brzezinski

The phosphomimetic mutation S82D in the cancer-associated, FAD-dependent human NADP(H):quinone oxidoreductase 1 (hNQO1) causes a decrease in flavin-adenine dinucleotide-binding affinity and intracellular stability. We test in this work whether the evolutionarily recent neutral mutation R80H in the vicinity of S82 may alter the strong functional effects of S82 phosphorylation through electrostatic interactions. We show using biophysical and bioinformatic analyses that the reverse mutation H80R prevents the effects of S82D phosphorylation on hNQO1 by modulating the local stability. Consistently, in rat NQO1 (rNQO1) which contains R80, the effects of phosphorylation were milder, resembling the behaviour found in hNQO1 when this residue was humanized in rNQO1 (by the R80H mutation). Thus, apparently neutral and evolutionarily divergent mutations may determine the functional response of mammalian orthologues towards phosphorylation.

Keywords: epistasis; flavoprotein; molecular evolution; protein phosphorylation

There are about 100 human proteins that depend on flavin nucleotides [mostly flavin-adenine dinucleotide (FAD) and flavin-mononucleotide (FMN)] for their catalytic function [1]. Most catalyse oxidation reactions involved in metabolic processes, in which the

flavin cofactor plays a critical role [1]. Flavin binding also controls flavoprotein intracellular stability by modulating the levels of degradation-prone flavin-free species (i.e. the apoprotein) [2–5]. Whether flavin binding simply leads to global thermodynamic stabilization of

Abbreviations

CTD, C-terminal domain; FAD, flavin-adenine dinucleotide; FMN, flavin-mononucleotide; HDXMS, hydrogen–deuterium exchange monitored by mass spectrometry; hNQO1, human NADP(H):quinone oxidoreductase 1; K_d , dissociation constant; k_{prot} , second-order rate constant for proteolysis; MD, molecular dynamics; NQO1_{apo}, ligand-free NQO1; NQO1_{dic}, FAD-dicoumarol-bound NQO1; NQO1_{holo}, FAD-bound NQO1; NTD, N-terminal domain; rNQO1, rat NADP(H):quinone oxidoreductase 1; TCS, thermolysin cleavage site; $\Delta\Delta G$, change in the free energy change between two states (e.g. mutant and WT protein).

the native state or increases the local stability of initiation sites for degradation is still a matter of debate [2,6,7,8]. Nearly 2/3 of human flavoproteins are associated with genetic diseases due to single amino acid exchanges (i.e. caused by missense mutations) [1,6,8,9,10]. In addition, it is likely that flavin-binding affinity (and consequently *in vivo* stability of flavoproteins) can be modulated by post-translational modifications such as phosphorylation, although our knowledge on this matter is very limited [3]. In this regard, we have recently reported that site-specific pseudophosphorylation at position S82 of the human NQO1 flavoenzyme [NADP(H):quinone oxidoreductase 1; EC 1.6.5.2; human NADP(H):quinone oxidoreductase 1 (hNQO1)] has dramatic effects on FAD-binding affinity and reduces intracellular protein levels.

Human NADP(H):quinone oxidoreductase 1 (hNQO1) is a multifunctional stress protein involved in both enzymatic and nonenzymatic functions, including the detoxification of quinones, activation of cancer prodrugs, stabilization of transcription factors such as p53 and p73 α upon direct physical interaction with them, and in other regulatory protein:protein and protein:RNA interactions (E. T. Salido, D. J. Timson, I. Betancor-Fernández, R. Palomino-Morales, & A. L. Pey, under review) [11–15]. Altered hNQO1 expression and activity are associated with different pathologies, including cancer and several neurological disorders (e.g. Parkinson's and Alzheimer's diseases) [2,8,12,15,16,17,18]. The enzyme forms functional homodimers, with two domains per monomer: an N-terminal domain (NTD, residues 1–224), that contains most of the binding site for FAD and the monomer:monomer interface, and a C-terminal domain (CTD; residues 225–274) which is involved in dimer stabilization and completes the binding sites for NADH and the substrates [12,19,20,21,22,23]. FAD binding is essential for the catalytic activity of hNQO1, acting as two-electron donor and acceptor during the catalytic cycle [8,24]. In addition, the high affinity for FAD [with a dissociation constant (K_d) in the 10–20 nM range] [25–27] and the adequate supply of riboflavin as precursor of FAD contribute to maintain the levels of the degradation-prone, highly flexible and partially unfolded apoprotein at low levels, thus controlling hNQO1 intracellular degradation rates [2,4,28]. Accordingly, the single amino acid exchange P187S and phosphorylation at the S82 site reduce 10- to 40-fold FAD-binding affinity with a concomitant effect on hNQO1 steady-state levels intracellularly [2,19,20,25]. Phosphorylation at position S82 is highly conserved across mammalian NQO1 sequences, as well as at the adjacent residues in the sequence, with a few exceptions (particularly residue 80; Fig. 1A). This phosphorylation event has been reported in 14 different

analyses of the flavoproteome (<https://www.phosphosite.org/proteinAction.action?id=14721&showAllSites=true>). The phosphomimetic mutation S82D destabilizes this region (particularly the region comprising residues 50–90) both in the holo- and apo-states of hNQO1, and this effect propagates to the FAD-binding site severely reducing its affinity for the flavin [3]. Importantly, this region contains a network of highly conserved ionizable residues that are likely responsible for the effects of S82D on FAD binding (Fig. 1B,C). Among these charged residues, the most noticeable exception is H80 in the human sequence vs the consensus sequence (Fig. 1C). The consensus amino acid at this position is R80 (Fig. 1C) engages in favourable interactions with neighbouring charged residues [27]. Consequently, the mutation H80R stabilizes this region in hNQO1, and the presence of R80 in most mammalian sequences (for instance, rat NQO1) may cause a similar effect. Although the H80R mutation has nearly neutral effects on hNQO1 (for instance on its binding affinity for FAD), it is capable of overcoming the effect of P187S on FAD-binding affinity through epistatic effects [26,27,29]. Therefore, we hypothesize that the mutations H80R and S82D may cause their opposing effects on FAD-binding affinity through charge–charge interactions acting on the same electrostatic network in the NTD. In this context, we propose that: (a) the presence of the H80R in hNQO1 would overcome the effects caused by the phosphomimetic mutation S82D on FAD-binding affinity; (b) since R80 is present in most of mammalian NQO1 sequences, although the phosphorylation of S82 may occur in these proteins, their effects would be modulated by the presence of R80 in close proximity. To test these proposals, we carried out structural and functional comparative analyses on hNQO1 and rat NQO1 (rNQO1). Our results supported that, due to the evolutionary divergence at residue 80, the phenotypic manifestation of phosphorylating S82 largely diverges between these highly similar orthologues.

Materials and methods

Protein expression and purification from *Escherichia coli*

Site-directed mutagenesis to introduce the S82D mutation was carried out on the pET-46 Ek/LIC containing hNQO1 H80R sequence as described earlier [25,27] and using the QuikChange lightning kit (Agilent Technologies, Madrid, Spain). Mutagenesis was confirmed by sequencing the entire cDNA. The cDNA of rNQO1 was synthesized and subcloned into the pET-15b vector by GenScript (Leiden,

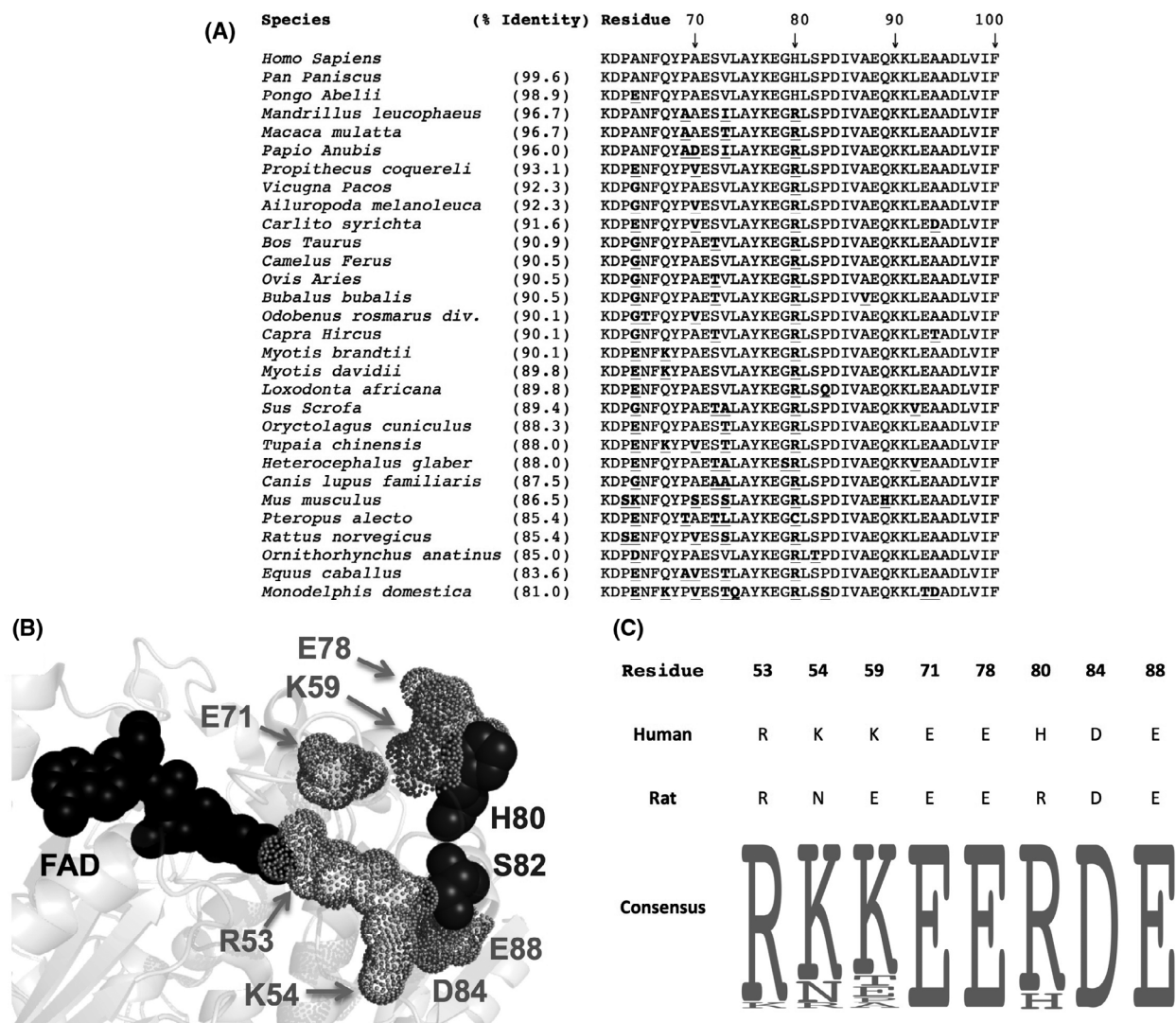


Fig. 1. Sequence conservation and structural features in the proximity of the H80 and S82 sites. (A) Sequence alignment of the region comprising residues 61–100 in hNQO1 and those of mammalian orthologous proteins. Residues in bold and underlined indicate nonidentical sites vs hNQO1. (B) Structural location of H80 and S82 in the hNQO1 structure regarding the FAD cofactor is shown as black spheres (PDB code: 1D4A) [22]. Ionizable residues that can interact with H80/R80 and/or S82/D82 residues and affect FAD binding are indicated in grey. (C) Frequency of sequence conservation of ionizable residues shown in panel B from the alignment of mammalian sequences displayed in panel (A). The consensus sequence is indicated as large letters and frequency indicated as the size of the letter. Figure reproduced from Ref. [22].

The Netherlands) and used as template to generate by site-directed mutagenesis in rNQO1 the mutants R80H, S82D and R80H-S82D. Expression and purification of wild-type (WT) and mutants from *Escherichia coli* BL21 (DE3), as well as preparation of apoproteins (using a KBr/urea-based procedure), were carried out as previously described [3]. Purified proteins were exchanged to 50 mM HEPES (2-[4-(2-hydroxyethyl)piperazin-1-yl]ethanesulfonic acid)-KOH at pH 7.4 and stored at -80°C upon flash-freezing in liquid N_2 . Along this manuscript, we refer to apoproteins [ligand-free NQO1 (NQO1_{apo})] for those NQO1 samples in which FAD was stripped and holoproteins [FAD-bound

NQO1 (NQO1_{holo})] for those in which proteins were incubated with a large excess of FAD (typically 100 μM).

Titration with FAD

Flavin-adenine dinucleotide-binding studies were carried out by fluorescence titrations of NQO1_{apo} with FAD as described in Ref. [30]. Both hNQO1_{apo} and rNQO1_{apo} proteins (at a 0.25 μM concentration) were titrated in 20 mM potassium phosphate at pH 7.4 (or in 50 mM HEPES-KOH, see Table S1) at 25 $^{\circ}\text{C}$ for at least 10 min. Fluorescence emission spectra were recorded in the 340–360 nm

range (excitation at 280 nm) using 5 nm slits, at a 200 nm·min⁻¹ scan rate and averaged over 10 consecutive scans. Plots of intensity at 350 nm vs total FAD concentration were used to obtain K_d (K_d values) upon fitting by using a single site binding model [27]. Experiments were replicated at least twice for each variant.

Proteolysis

Kinetic proteolysis studies by thermolysin were performed in 50 mM HEPES-KOH, 10 mM CaCl₂ at pH 7.4 and 25 °C, as recently described [27,28]. hNQO1_{apo} protein variants were used at 10–20 μM concentration, with an excess of 100 μM FAD, and experiments were carried out using a concentration of 0.01–0.8 μM in thermolysin. Proteolysis was initiated by addition of the protease, and samples were withdrawn at different times and quenched by adding a final concentration of 25 mM EDTA at pH 8. Samples were denatured with Laemmli's buffer and analysed by polyacrylamide gel electrophoresis in the presence of SDS (SDS/PAGE) containing 12% acrylamide. Gels were scanned and analysed using the IMAGEJ software (<https://imagej.nih.gov/>). Time-dependent decay of uncleaved NQO1 was used to determine first-order rate constants (k_{obs}) from fittings carried out using an exponential function. Second-order rate constants (k_{prot}) were obtained by dividing first-order rate constants by the protease concentration used.

Double-mutant cycles

Thermodynamic double-mutant cycles were built using data from proteolysis kinetics (k_{prot}) and FAD-binding affinities (K_d). These cycles allowed us to determine thermodynamic effects of mutations from variations in relevant free energies ($\Delta\Delta G$) for proteolysis or FAD binding between protein variants. For proteolysis kinetics, $\Delta\Delta G_{\text{prot}(A-B)} = R \cdot T \cdot \ln \frac{k_{\text{prot}(B)}}{k_{\text{prot}(A)}}$ where $k_{\text{prot}(i)}$ values were the corresponding second-order proteolysis rate constants, R was the ideal gas constant (1.987 cal·mol⁻¹·K⁻¹), and T was the experimental absolute temperature. Since the k_{prot} was determined under conditions at which the proteolytic step was rate-limiting [28,31], and both A and B species (e.g. WT vs a mutant) were cleaved at the same site, the ratio $\frac{k_{\text{prot}(B)}}{k_{\text{prot}(A)}}$ can be considered equal to the ratio of the equilibrium constant between cleavable (X) and native states (N) for the A and B species (e.g. WT and a mutant). A positive value of $\Delta\Delta G_{\text{prot}(A-B)}$ indicates that A has higher stability than B (i.e. A has a lower equilibrium constant; $K = \frac{[X]}{[N]}$ the population of X is lower for A than for B). For FAD binding, $\Delta\Delta G_{\text{binding}(A-B)} = R \cdot T \cdot \ln \frac{K_d(B)}{K_d(A)}$ where K_d is the dissociation constant for FAD binding for species A and B, respectively. A positive value of $\Delta\Delta G_{\text{binding}(A-B)}$ indicates that the state A binds FAD more tightly than B (i.e. A has

lower K_d than B). Errors associated with $\Delta\Delta G$ were determined by propagation of fitting errors.

Hydrogen/deuterium exchange mass spectrometry

Amide hydrogen/deuterium exchange (HDX) of NQO1 was investigated for hNQO1 variants in the NQO1_{apo} and NQO1_{holo} forms essentially as described in Ref. [32]. Briefly, the exchange reaction was initiated by a 10-fold dilution of 20 μM protein with a D₂O-based buffer containing 50 mM HEPES-KOH, pD 7.4, 0.5 mM tris(2-carboxyethyl) phosphine. The exchange was terminated at different points as described in Ref. [32]. Custom-made columns coupled in tandem were used for proteolysis that was done at 0 °C by 0.4% formic acid in water [32]. The generated peptides were desalted on a SecurityGuard™ precolumn (ULTRA Cartridges UHPLC Fully Porous Polar C18, 2.1 mm, Phenomenex, Torrance, CA, USA) using the same solvent and flow that were used for digestion. Solvent was delivered by using a 1260 Infinity II Quaternary pump (Agilent Technologies, Waldbronn, Germany). Peptides were further separated on an analytical column (LUNA® Omega Polar C18 Column, 100 Å, 1.6 μm, 100 mm × 1.0 mm; Phenomenex) by linear gradient (10–40% buffer B in 6 min; buffer B contained 0.1% FA/98% ACN in water) followed by a quick step to 99% B lasting 5 min. Solvent delivery on the analytical column was managed as described in Ref. [32]. Digestion, desalting and separation were performed at 0 °C and pH 2.3 to minimize deuterium back-exchange. The outlet of the column was online connected to an ESI source of 15T FT-ICR mass spectrometer (Bruker Daltonics, Bremen, Germany) operating in broad-band positive ion MS mode. Data were exported using DATAANALYSIS 5.0 (Bruker Daltonics) and processed by in-house developed program Deutex (unpublished). Peptide identification was done in a separate data-dependent LC-MS/MS run. Data were exported to mgf files using DATAANALYSIS 5.0 and searched against database containing sequences of NQO1 variants, proteases used in the experiment and common contaminating proteins (cRAP database). As a semiquantitative measurement of the HDX kinetic differences between hNQO1 variants and/or ligation states, we used $\Delta\%D_{\text{av}}$ that is calculated from the three most different values in HDX kinetics between a given state and the reference state [32].

Molecular dynamics simulations

Molecular dynamics (MD) of dimeric hNQO1 was performed by using the GROMACS package [33], largely following a protocol previously applied [3]. Eight simulation runs were carried out, differing by the absence or presence of (a) the FAD cofactor (apo- and holo states, respectively); (b) the suppressor mutation H80R; and (c) the phosphomimetic

mutation S82D. The protein structures were built starting from the crystallographic structure of the holoprotein (PDB entry 1D4A [22]). The addition of a few missing atoms and residue modifications at the mutation sites were carried out *in silico* by using visual MD (VMD) [34].

The protein was solvated in a rhombic dodecahedron box with a minimum distance of 1 nm from each wall, resulting in ~17 800 water molecules, and Cl⁻ counterions were added to obtain an overall neutral system charge. Classical MD was performed with periodic boundary conditions in the isothermal-isobaric ensemble, using the AMBER force field 99SB-ILDN for the protein [35], the generalized AMBER force field (GAFF) for FAD [36], and the TIP3P model for water [37]. Other conditions, including reference values and coupling times for the thermostat and barostat, modelling of nonbonded Coulomb and van der Waals interactions, and distance constraints on bonds, were as previously described [38,39]. Each simulation run was carried out with a sampling time of 1 ps, for a total time of 100 ns.

The structural and dynamic properties of hNQO1 were assessed by calculating atomic deviations and fluctuations in the protein structure, after rototranslation with a least squares fit to the C^α atoms with respect to the starting conformation to account for protein diffusion. Equilibration of protein inner motion was assessed by monitoring the root mean square deviations (RMSDs) of C^α atoms; 10 ns was typically sufficient for the NQO1_{holo}, and further analysis was carried out in the 20- to 100-ns time interval for ensuring a complete equilibration in all the cases. For all simulations, values for RMSDs and for root mean square fluctuations (RMSFs) were calculated as averages on both protein monomers, and the two outmost residues at the N and C termini of the protein chains were excluded in the analysis due to their high mobility.

Electrostatic calculations were carried out using the solvent-accessibility corrected Tanford–Kirkwood model [40] as recently described [27] taking as input the average structures from the last 80 ns of the MD simulations. The output of these analyses provided the energy of charge–charge interactions of a given ionizable residue with all the individual ionizable amino acids in the protein dimer (E_{q-q}) and was averaged for each ionizable residue.

Results and Discussion

The mutation H80R protects hNQO1 against the effects of S82D on FAD binding without affecting interaction with SAMp73

To prove whether H80R may protect hNQO1 towards the most deleterious effect known for the phosphomimetic mutation S82D (i.e. the affinity for FAD) [3], we produced and purified hNQO1 WT, the single mutants H80R and S82D and the double-mutant

H80R-S82D, and characterized their affinity for FAD. It is worth noting that the introduction of these mutations on hNQO1 did not affect the overall dimeric structure of hNQO1_{holo} and hNQO1_{apo} states (Figs S1 and S2). Titrations of hNQO1 variants were carried out in phosphate buffer to obtain accurate measurements for high-affinity variants (according to Ref. [26]) and provide results also consistent with those in HEPES buffer (Table S1) [3,27]. Under these conditions, we observed a mild increase in affinity for FAD in H80R whereas the S82D mutant showed a decrease in FAD-binding affinity by 11-fold (Fig. 2A). Importantly, the interaction between H80R and S82D basically restored the affinity for FAD to that of hNQO1 WT (Fig. 2A).

To support that the interaction between H80R and S82D overcomes the local destabilization of the phosphomimetic mutation in the vicinity of the FAD-binding site (residues 50–90) [3,27], we carried out comparative analysis of the resistance of NQO1_{holo} proteins against proteolytic cleavage by thermolysin. The initial cleavage by thermolysin occurs in hNQO1_{holo} WT (as well as in the H80R, S82D and H80R-S82D mutants; see Fig. S3) between S72 and V73 (named the thermolysin cleavage site; TCS) leading to the accumulation of a cleavage intermediate of ~22.8 kDa (see Fig. S3) [28]. The TCS is half-way between the mutated sites in H80R and S82D and the FAD molecule (with shortest distances of 6.4, 7.5 and 10 Å, respectively; Fig. 2B) and thus allows to correlate the changes in the local stability due to these mutations and their propagation to the FAD-binding site [3,27]. Proteolysis experiments were carried out under conditions in which the proteolysis rate constants depended linearly on protease concentration, and thus, the second-order proteolysis rate constants (k_{prot}) reported the effect of mutations on the thermodynamic local stability of the TCS (Fig. S2B–D) [41,42].

The mutations H80R and S82D had clear effects on the local stability of the TCS, causing a five-fold decrease and a 30-fold increase in k_{prot} , respectively. This indicates an important stabilization for H80R and destabilization for S82D around this region (Fig. 2B). Remarkably, the interaction between these two mutations in the H80R-S82D mutant essentially restored the local stability of the TCS to that observed in the WT protein (Fig. 2B). These results thus support that the mutation R80H that occurred about 20 Myr ago [27] might have made hNQO1 more sensitive to the phosphorylation effects at S82.

The quantitative analyses reported here for the effects of the mutations H80R and S82D on hNQO1, and their interaction, allowed us to build double-mutant

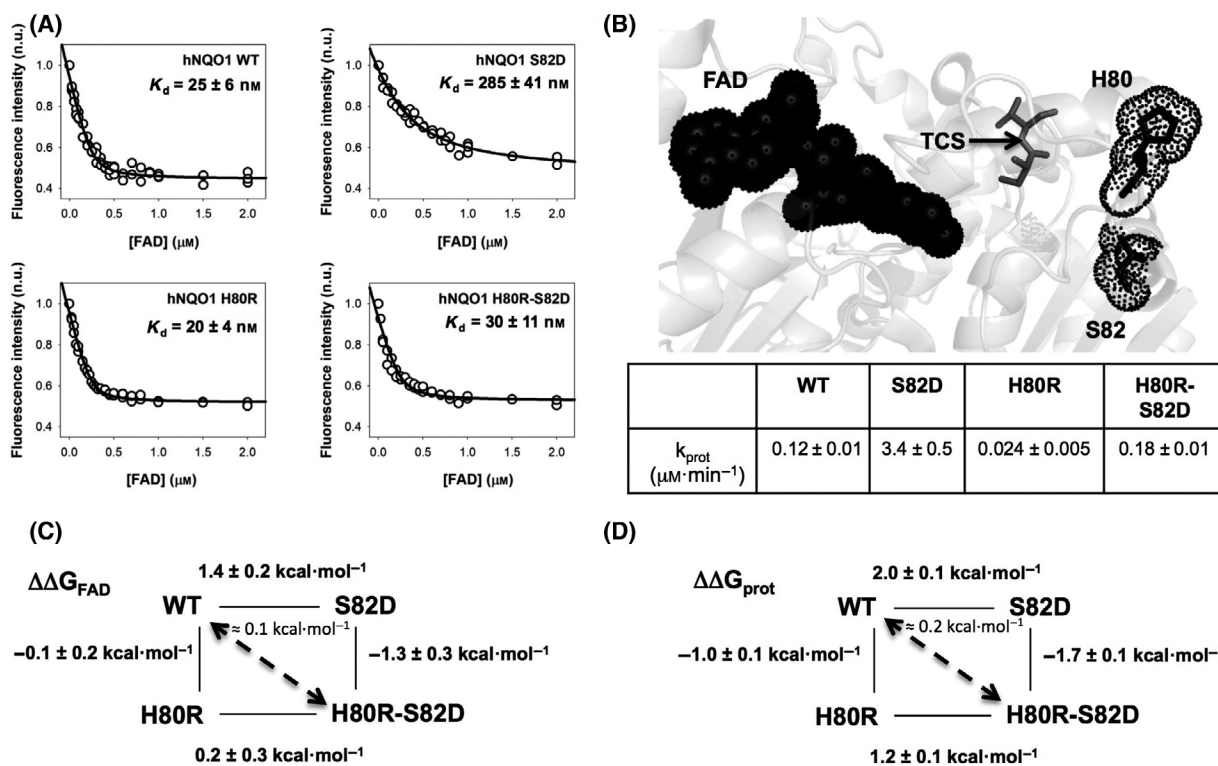


Fig. 2. Effects of the mutations S82D and H80R on the affinity for the FAD as hNQO1_{apo} proteins and local stability of the NTD as hNQO1_{holo} proteins from proteolysis kinetics. (A) Titrations of hNQO1_{apo} variants with FAD. Fluorescence intensity was normalized using that of the apoprotein in the absence of FAD. Data are from 2 to 3 independent titrations. K_d values were determined by using a single type of independent binding site model. Protein concentration was $0.25 \mu\text{M}$. (B) Proteolysis kinetics by thermolysin. The upper panel shows the location of the H80 and S82 residues regarding the TCS and the FAD molecule (PDB code: 2F1O) [46]. The table shows the second-order proteolysis rate constants (k_{prot}) for hNQO1_{holo} variants. (C, D) Double-mutant cycles for FAD-binding affinity (C) and proteolysis (D, for NQO1_{holo} variants). The diagonal arrows indicate the approximate change in ΔG from WT and double mutant as initial and final states. All experiments were performed at 25°C . Figure reproduced from Ref. [46].

cycles to evaluate their effects on FAD-binding affinity and local stability of the TCS (Fig. 2C,D). The first point to note is the existence of epistasis between these two mutations (i.e. the effect of a given mutation depends on the presence or absence of the other mutation) (Fig. 2C,D). It is evident that the H80R mutation shows stronger effects in the presence of the S82D mutation, whereas the effect of the S82D mutation is much milder in the presence of the H80R mutation (Fig. 2C,D). Additionally, the double-mutant cycles revealed similar effects on FAD-binding affinity and the stability of the TCS, although some quantitative differences beyond the experimental uncertainty were observed. This can be easily rationalized because FAD-binding affinity should depend on the effects of mutations on the conformational landscape of hNQO1_{holo} and hNQO1_{apo} (i.e. the FAD-binding site). In contrast, proteolysis kinetics by thermolysin only reports on the effects on hNQO1_{holo} (note that proteolysis on

hNQO1_{apo} does not unambiguously reports on the stability of the TCS) [28]. We also compared the average change in TCS stability and FAD binding, going from WT to the H80R-S82D using both pathways (either S82D or H80R as intermediate) with the actual $\Delta\Delta G$ change observed between H80R-S82D and the WT protein. In both cases, the double mutants show virtually the same $\Delta\Delta G$ values (diagonal arrows in the cycles; Fig. 2).

A critical function of hNQO1 is its interaction with protein partners (such as p73 α) that depends to some extent to the catalytic competence of the protein (E. T. Salido, D. J. Timson, I. Betancor-Fernández, R. Palomino-Morales, & A. L. Pey, under review) [19,27,43]. Previous studies have shown that the single mutations H80R and S82D lead to certain differences in the interaction of hNQO1 with SAMP73 α , as observed by NMR spectroscopy experiments [3,19,27]. However, the mutant H80R-S82D showed little perturbation of

the set of residues in SAMp73 α upon interaction with hNQO1 (Fig. S4).

High-resolution structural characterization of the interaction between H80R and S82D in hNQO1

To determine at high resolution the mechanism by which the interaction of the mutation H80R with S82D leads to structural stabilization of the FAD-binding site, we first determined the effects of these single mutations and their combination on the local stability of hNQO1_{holo} and hNQO1_{apo} by hydrogen–deuterium exchange monitored by mass spectrometry (HDXMS) [32] (Fig. 3). Since HDX occurs under the EX2 regime (in which the intrinsic exchange rate constant k_{int} is much lower than the rate constant k_{cl} for the conversion between nonexchanging and exchanging states, according to the Linderström-Lang model) [44], changes due to ligand binding and/or mutations report changes in local thermodynamic stability for the different protein segments [32]. It must be noted that the kinetic behaviour under HDX conditions is very complex and heterogeneous for the hNQO1 protein, and thus, a direct analysis of ligand binding and mutational effects on local stability from HDX kinetics is not straightforward (see [32] for a detailed Discussion; Figs S5–S8). Therefore, to compare the effects of the H80R and S82D mutations on the local stability of hNQO1_{holo} and hNQO1_{apo}, we determined $\Delta\% D_{\text{av}}$ values for different segments (Figs S5–S8), as a simple metric that describes semiquantitatively changes in HDX kinetics [32]. Please note that a positive value of $\Delta\% D_{\text{av}}$ indicates destabilization vs. the reference state, while a negative value indicates stabilization (Fig. 3).

In the hNQO1_{holo} state, the mutation S82D caused significant structural destabilization of the NTD in the regions involving residues 50–90 and 100–120, and this effect is particularly strong in the segments 69–74 and 110–113 (in agreement with a recent report) [30], whereas the mutation H80R strongly stabilizes the segment 50–90 (Fig. 3A and Fig. S5). Remarkably, for the double-mutant H80R-S82D, the effects of the single mutations on the segments 50–90 essentially cancel out (Fig. 3A and Fig. S5). Analogous analyses of the hNQO1_{apo} state reveal a similar, but more complex, scenario (also in agreement with a recent report) [30]. The mutation S82D destabilizes segments 50–90 and 100–140, although to a lower extent than for the hNQO1_{holo} state. The mutation H80R stabilizes the segments 50–90 to a similar extent than that observed for the NQO1_{holo} state, and this stabilization is also observed in segments 50–90 and 100–120. The double-mutant H80R-S82D showed a behaviour half-way between of those of H80R and S82D (Fig. 3A and Fig.

S5). Interestingly, the mutations H80R and S82D also cause some mild long-range effects on the stability of the CTD in the NQO1_{apo} state (Fig. 3A and Fig. S5).

Since the regions in the NTD whose stabilities are affected by the mutations S82D and H80R are in the vicinity of the FAD-binding site, these effects on structural stability might translate into changes in the FAD-binding affinity. This correlation is evident when we compare the effect of these two mutations on the structural stability of the FAD-binding site (i.e. those residues in direct contact with the flavin cofactor in the crystal structure; [32]). Interestingly, we found that the mutation S82D significantly reduces the stability of the FAD-binding site, both in the NQO1_{holo} and NQO1_{apo} states, whereas the effects of the mutation H80R are marginal (Fig. 3B). The interaction between the mutations H80R and S82D on the double mutant essentially abolished the deleterious effects of S82D on the FAD-binding site (Fig. 3B). Importantly, the effects of the single mutations and their combination in the double mutant seem to be stronger on hNQO1_{holo}, thus explaining the good correlation found in the double-mutant cycles.

It is likely that alterations in electrostatic interactions in the NTD caused by the mutations H80R and S82D are largely responsible for the functional rescue in the double mutant through structural stabilization of the FAD-binding site and its surroundings. However, we might expect that the presence of R80 and D82 in the double mutant alters the local electrostatic environment beyond their simple binary electrostatic interaction (see Fig. 1A). For instance, our HDXMS studies together with previous structural data indicate that the mutation H80R may alter the electrostatic interactions of this residue with certain neighbouring residues, particularly K59, E71 and E78, and consequently the local stability [27,29]. As we pointed out earlier, most of the residues involved on this electrostatic network are well conserved among mammalian sequences, the main exception being H80 (Fig. 1B,C). To further characterize these effects in the local electrostatic network, we calculated changes in electrostatic energies upon introduction of the H80R and/or S82D mutations on the averaged structures provided by MD simulations. These changes mostly localized around the mutated residues in the MD simulations (i.e. they were local) and mostly involved ionizable residues in the region comprising residues 50–90 (Fig. 4A and Fig. S9). Introduction of the single mutations H80R and S82D on the hNQO1_{holo} and hNQO1_{apo} states had opposing effects, leading to favourable and unfavourable electrostatic interactions with neighbouring residues, respectively (Fig. 4A). When both the H80R and S82D were present, we observed some (but not full) compensation of their

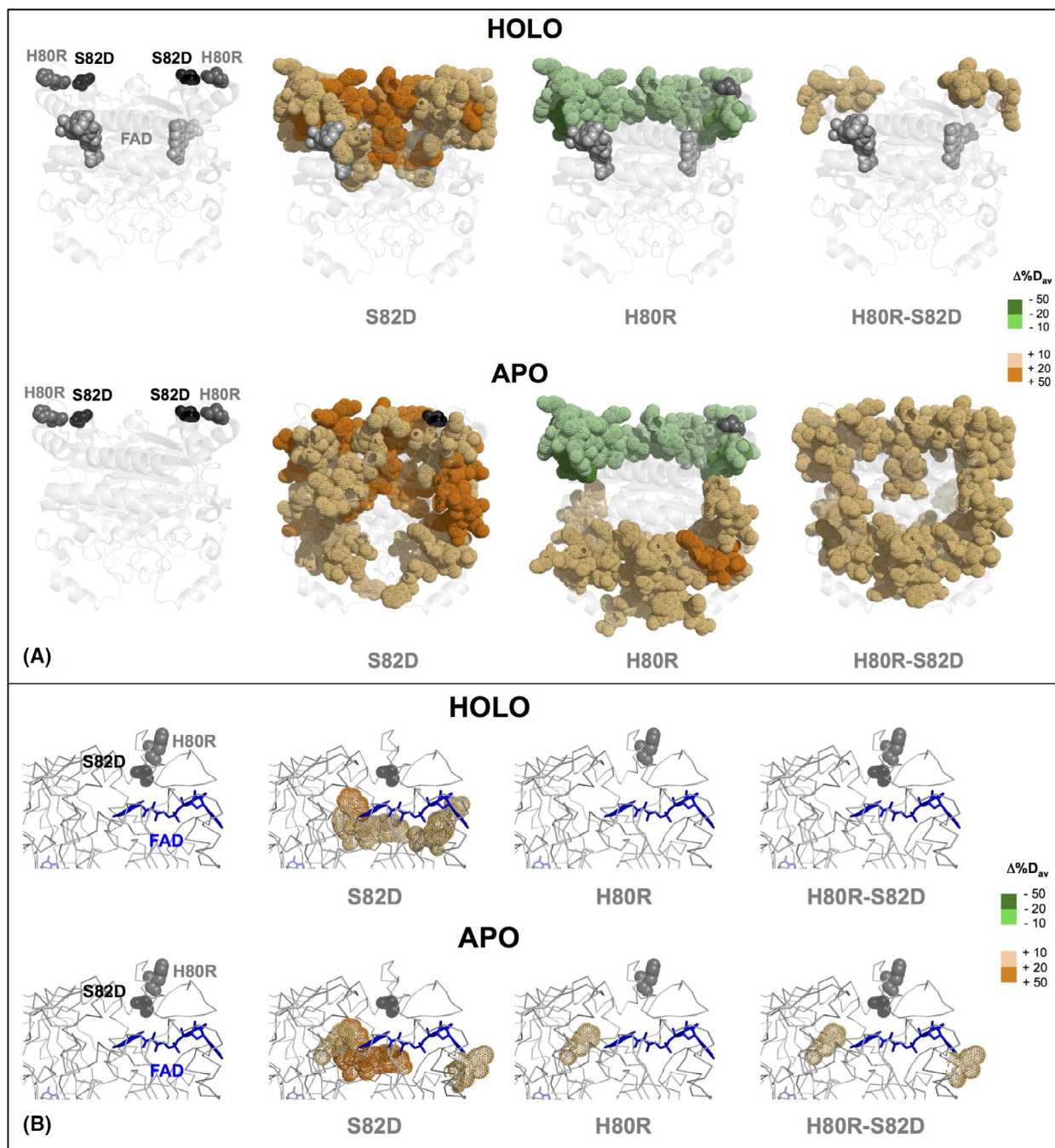


Fig. 3. Effects of the mutations H80R and S82D on the structural stability of hNQO1 as determined by HDXMS. The figure shows a structural representation of the effect of S82D and H80R and its combination in the hNQO1 protein as holo- and apoprotein. Residues depicted in the orange (destabilizing) and green (stabilizing) indicate those whose stability differs from the WT protein (as determined by $\Delta\%D_{av}$ values). Panel (A) shows these stability effects for the hNQO1 dimer, whereas panel (B) shows a close-view of those residues that form the FAD-binding site according to Ref. [32]. Figure reproduced from Ref. [32].

effects on electrostatic interactions in both ligation states. These analyses agreed well with those derived from HDXMS studies (Fig. 4B).

Additionally, the single mutations H80R and S82D also led to modest changes in the conformation and dynamics in the vicinity of the FAD-binding site (Fig.

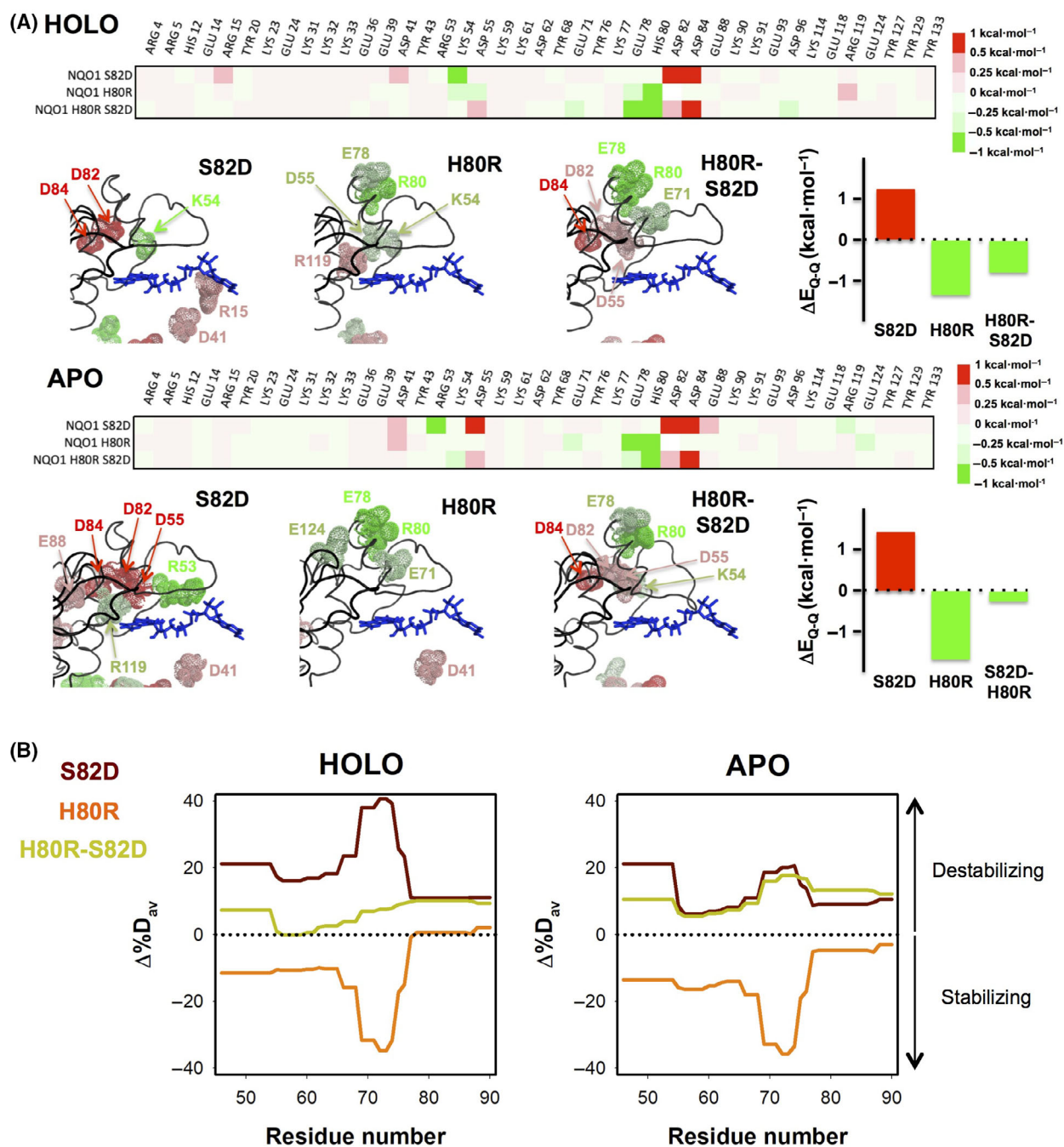


Fig. 4. An evolutionarily conserved electrostatic network mediates the effect of mutations H80R and S82D on the stability of the NTD. (A) Changes in electrostatic interactions derived from MD simulations. The colour maps showed the changes in electrostatic energy using the WT structure as reference (ΔE_{q-q}) for the ionizable residues in the N-terminal half of NQO1 (for the results showing the full length protein, see Fig. S9). Changes larger than $0.25 \text{ kcal}\cdot\text{mol}^{-1}$ in the vicinity of the FAD molecule were mapped onto the structure of the S82D, H80R and H80R-S82D variants. Bar plots in the right side showed the total effect of the residues highlighted in the structures. Colour scales indicated the ΔE_{q-q} for colour maps and structural displays. Positive values indicate destabilizing and negative values stabilizing effects, respectively. (B) HDXMS analysis shows that this network of electrostatic interactions mostly involving residues 45–90 in the NTD leads to changes in local stability. $\Delta\%D_{av}$ refer to changes in stability vs hNQO1 WT.

S10). The effects on the conformation were more noticeable for hNQO1_{apo} than for hNQO1_{holo}, and remarkably important near the loops 58–67, previously shown to be key for explaining the effects of the mutations H80R and S82D on FAD binding [3,29] (Fig. S10A–C,E,F). In the double mutant, we observed that the effect of the mutations on the conformation of the FAD-binding site largely (but not fully) cancelled out in hNQO1_{apo} (Fig. S10D–G). This would contribute to explain the compensatory effect of the H80R mutation on the S82D mutation regarding FAD binding to hNQO1. The mutation H80R also reduced the dynamics in the vicinity of the FAD-binding site in hNQO1_{apo}, which may reflect stabilization of FAD-binding competent states, whereas the S82D mutation caused much milder effects (Fig. S10E,F). Again, these effects on dynamics largely cancelled out in the hNQO1_{apo} in the double mutant, thus suggesting that this cancellation of effects could contribute to their compensatory behaviour on FAD-binding affinity.

Overall, these analyses combining HDXMS and MD simulations supported that electrostatic interactions

modulate the local stability, conformation and dynamics in the vicinity of the FAD-binding site, and these effects are key to explain the opposing effects of S82D and H80R on the binding affinity of NQO1 for the flavin cofactor and their compensation in the double-mutant H80R-S82D.

Rat NQO1 is resistant to the effects of S82D due to the mutation R80

We would expect that mammalian orthologues containing R80 would be less sensitive to the phosphomimetic mutation S82D. To test this hypothesis, we purified rat NQO1 (rNQO1) that contains R80 (see Fig. 1C) as well as rNQO1 containing the mutation S82D, and two humanized versions in which the mutation R80H was introduced with or without the mutation S82D, and determined their affinity for FAD (Fig. 5). The mutation S82D had much weaker effect on rNQO1 (two-fold decrease in affinity) than in hNQO1 (11-fold decrease in affinity). The humanizing mutation R80H in rNQO1 reduced the affinity for

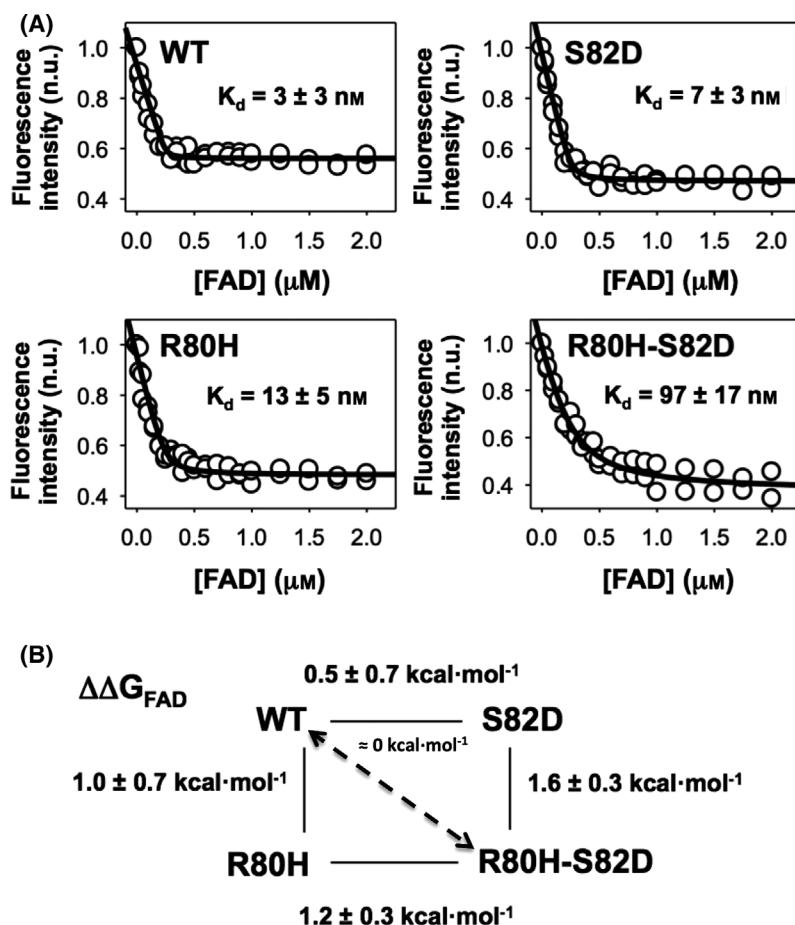


Fig. 5. Effects of the S82D and R80H mutations on the affinity for the FAD of rNQO1_{apo} proteins. (A) Titrations of apo-rNQO1 variants with FAD. Fluorescence intensity was normalized by using the intensity of the apoprotein in the absence of FAD. Data are from two independent titrations. K_d values were determined by fittings using a single type of independent binding sites. Protein concentration was $0.25 \mu\text{M}$. (B) Double-mutant cycles for FAD-binding affinity. The diagonal arrows indicate the approximate change in ΔG from WT and double mutant as initial and final states. Experiments were performed at 25 °C.

FAD to a value close to that of hNQO1. More importantly, when the humanizing mutation R80H was combined with the mutation S82D, we observed a 30-fold decrease in affinity vs WT rNQO1. Overall, these results strongly support that the mutation R80H that occurred about 20 Myr ago [27] has rendered NQO1 from some primates (including humans) sensitive to phosphorylation at position S82. This might represent a recent evolutionary change in the functional response of NQO1 due to phosphorylation, mainly due to the mutation R80H that occurred 20 Myr ago. Again, we compared the value of $\Delta\Delta G$ from two ways (Fig. 5). These results strongly support that our mutant cycles work well from the initial to the final state.

Conclusions

Along molecular evolution, proteins develop new functions and regulatory mechanisms through mutations [45]. We have previously shown that phosphorylation of hNQO1 at the residue S82 had large effects in FAD binding and intracellular stability [3], whereas the evolutionary divergent mutation R80H (that occurred during primate speciation about 20 Myr ago) is almost neutral for WT hNQO1 [27]. In this work, we showed that the interaction of S82D with H80R or the inverse mutation in hNQO1 and rNQO1 may have turned off/on evolutionarily shifted with a recently occurred single mutation. Our results showed that rNQO1 is not sensitive to phosphorylation at residue S82, but the single and humanizing mutation R80H makes rNQO1 sensitive to phosphorylation at this site. Overall, our results allow us to hypothesize that a single evolutionary-related mutation may switch on/off the effects of phosphorylation in protein function in many other proteins.

Acknowledgements

ALP thanks Professors José Manuel Sánchez-Ruiz and Beatriz Ibarra-Molero (both from the University of Granada) for providing access and advice on their home-built software for electrostatic calculations. BR acknowledges kind hospitality and use of computational resources in the European Magnetic Resonance Center (CERM), Sesto Fiorentino (Florence), Italy. This work was supported by Spanish Ministry of Economy and Competitiveness and European ERDF Funds (MCIU/AEI/FEDER, EU) [RTI2018-097991-B-I00 to JLN and RTI2018-096246-B-I00 to ALP]; FEDER/Junta de Andalucía-Consejería de Transformación Económica, Industria, Conocimiento y Universidades [Grant P18-RT-2413 to ALP]. Financial

support from EU Horizon 2020 project EU FT-ICR MS (731077) as well as institutional (CZ.1.05/1.1.00/02.0109) and MS facility support (LM2018127 CIISB) are gratefully acknowledged. Funding for open charge: Universidad de Granada/CBUA.

Author contributions

ALP was responsible for conceptualization. ALP, BR, RG, JLN, DK and PM were responsible for methodology. JLP-G, ALP, DL, PV, BR, DK, RG, NM-T and JLN carried out the investigation and analysed data. ALP, JLN, PM and ALP wrote the initial draft, and all authors contributed to write and edit the final version.

Data accessibility

The data that support the findings of this study are contained in the figures and in the supplementary material of this article. Any material is available from the corresponding author upon reasonable request.

References

- Lienhart WD, Gudipati V and Macheroux P (2013) The human flavoproteome. *Arch Biochem Biophys* **535**, 150–162.
- Martinez-Limon A, Alriquet M, Lang WH, Calloni G, Wittig I and Vabulas RM (2016) Recognition of enzymes lacking bound cofactor by protein quality control. *Proc Natl Acad Sci USA* **113**, 12156–12161.
- Medina-Carmona E, Rizzuti B, Martin-Escolano R, Pacheco-Garcia JL, Mesa-Torres N, Neira JL, Guzzi R and Pey AL (2019) Phosphorylation compromises FAD binding and intracellular stability of wild-type and cancer-associated NQO1: insights into flavo-proteome stability. *Int J Biol Macromol* **125**, 1275–1288.
- Moscovitz O, Tsvetkov P, Hazan N, Michaelevski I, Keisar H, Ben-Nissan G, Shaul Y and Sharon M (2012) A mutually inhibitory feedback loop between the 20S proteasome and its regulator, NQO1. *Mol Cell* **47**, 76–86.
- Nagao M and Tanaka K (1992) FAD-dependent regulation of transcription, translation, post-translational processing, and post-processing stability of various mitochondrial acyl-CoA dehydrogenases and of electron transfer flavoprotein and the site of holoenzyme formation. *J Biol Chem* **267**, 17925–17932.
- Lucas TG, Henriques BJ and Gomes CM (2020). Conformational analysis of the riboflavin-responsive ETF:QO-p.Pro456Leu variant associated with mild multiple acyl-CoA dehydrogenase deficiency. *Biochim Biophys Acta Proteins Proteom* **1868**, 140393.

- 7 Pey AL, Megarity CF and Timson DJ (2019) NAD(P)H quinone oxidoreductase (NQO1): an enzyme which needs just enough mobility, in just the right places. *Biosci Rep* **39**, BSR20180459.
- 8 Beaver SK, Mesa-Torres N, Pey AL and Timson DJ (2019) NQO1: a target for the treatment of cancer and neurological diseases, and a model to understand loss of function disease mechanisms. *Biochim Biophys Acta Proteins Proteom* **1867**, 663–676.
- 9 Henriques BJ, Lucas TG and Gomes CM (2016) Therapeutic approaches using riboflavin in mitochondrial energy metabolism disorders. *Curr Drug Targets* **17**, 1527–1534.
- 10 Ribeiro JV, Lucas TG, Bross P, Gomes CM and Henriques BJ (2020) Potential complementation effects of two disease-associated mutations in tetrameric glutaryl-CoA dehydrogenase is due to inter subunit stability-activity counterbalance. *Biochim Biophys Acta Proteins Proteom* **1868**, 140269.
- 11 Ross D and Siegel D (2017) Functions of NQO1 in cellular protection and CoQ10 metabolism and its potential role as a redox sensitive molecular switch. *Front Physiol* **8**, 595.
- 12 Pey AL, Megarity CF, Medina-Carmona E and Timson DJ (2016) Natural small molecules as stabilizers and activators of cancer-associated NQO1 polymorphisms. *Curr Drug Targets* **17**, 1506–1514.
- 13 Betancor-Fernandez I, Timson DJ, Salido E and Pey AL (2018) Natural (and unnatural) small molecules as pharmacological chaperones and inhibitors in cancer. *Handb Exp Pharmacol* **45**, 345–383.
- 14 Ben-Nissan G and Sharon M (2014) Regulating the 20S proteasome ubiquitin-independent degradation pathway. *Biomolecules* **4**, 862–884.
- 15 Ross D and Siegel D (2021) The diverse functionality of NQO1 and its roles in redox control. *Redox Biol* **41**, 101950.
- 16 Ross D and Siegel D (2018) NQO1 in protection against oxidative stress. *Curr Opin Toxicol* **7**, 67–72.
- 17 Lajin B and Alachkar A (2013) The NQO1 polymorphism C609T (Pro187Ser) and cancer susceptibility: a comprehensive meta-analysis. *Br J Cancer* **109**, 1325–1337.
- 18 Lastres-Becker I, Garcia-Yague AJ, Scannevin RH, Casarejos MJ, Kugler S, Rabano A and Cuadrado A (2016) Repurposing the NRF2 activator dimethyl fumarate as therapy against synucleinopathy in Parkinson's disease. *Antioxid Redox Signal* **25**, 61–77.
- 19 Medina-Carmona E, Neira JL, Salido E, Fuchs JE, Palomino-Morales R, Timson DJ and Pey AL (2017) Site-to-site interdomain communication may mediate different loss-of-function mechanisms in a cancer-associated NQO1 polymorphism. *Sci Rep* **7**, 44352.
- 20 Lienhart WD, Gudipati V, Uhl MK, Binter A, Pulido SA, Saf R, Zangger K, Gruber K and Macheroux P (2014) Collapse of the native structure caused by a single amino acid exchange in human NAD(P)H:quinone oxidoreductase(1). *FEBS J* **281**, 4691–4704.
- 21 Chen S, Deng PS, Bailey JM and Swiderek KM (1994) A two-domain structure for the two subunits of NAD(P)H:quinone acceptor oxidoreductase. *Protein Sci* **3**, 51–57.
- 22 Faig M, Bianchet MA, Talalay P, Chen S, Winski S, Ross D and Amzel LM (2000) Structures of recombinant human and mouse NAD(P)H:quinone oxidoreductases: species comparison and structural changes with substrate binding and release. *Proc Natl Acad Sci USA* **97**, 3177–3182.
- 23 Li R, Bianchet MA, Talalay P and Amzel LM (1995) The three-dimensional structure of NAD(P)H:quinone reductase, a flavoprotein involved in cancer chemoprotection and chemotherapy: mechanism of the two-electron reduction. *Proc Natl Acad Sci USA* **92**, 8846–8850.
- 24 Anoz-Carbonell E, Timson DJ, Pey AL and Medina M (2020) The catalytic cycle of the antioxidant and cancer-associated human NQO1 enzyme: hydride transfer, conformational dynamics and functional cooperativity. *Antioxidants (Basel)* **9**, 772.
- 25 Pey AL, Megarity CF and Timson DJ (2014) FAD binding overcomes defects in activity and stability displayed by cancer-associated variants of human NQO1. *Biochim Biophys Acta* **1842**, 2163–2173.
- 26 Claveria-Gimeno R, Velazquez-Campoy A and Pey AL (2017) Thermodynamics of cooperative binding of FAD to human NQO1: Implications to understanding cofactor-dependent function and stability of the flavoproteome. *Arch Biochem Biophys* **636**, 17–27.
- 27 Medina-Carmona E, Fuchs JE, Gavira JA, Mesa-Torres N, Neira JL, Salido E, Palomino-Morales R, Burgos M, Timson DJ and Pey AL (2017) Enhanced vulnerability of human proteins towards disease-associated inactivation through divergent evolution. *Hum Mol Genet* **26**, 3531–3544.
- 28 Medina-Carmona E, Palomino-Morales RJ, Fuchs JE, Padin-Gonzalez E, Mesa-Torres N, Salido E, Timson DJ and Pey AL (2016) Conformational dynamics is key to understanding loss-of-function of NQO1 cancer-associated polymorphisms and its correction by pharmacological ligands. *Sci Rep* **6**, 20331.
- 29 Munoz IG, Morel B, Medina-Carmona E and Pey AL (2017) A mechanism for cancer-associated inactivation of NQO1 due to P187S and its reactivation by the consensus mutation H80R. *FEBS Lett* **591**, 2826–2835.
- 30 Pacheco-Garcia JL, Anoz-Carbonell E, Vankova P, Kannan A, Palomino-Morales R, Mesa-Torres N, Salido E, Man P, Medina M, Naganathan AN *et al.* (2021) Structural basis of the pleiotropic and specific phenotypic consequences of missense mutations in the multifunctional NAD(P)H:quinone oxidoreductase 1

- and their pharmacological rescue. *Redox Biol* **46**, 102112.
- 31 Fuchs JE, Muñoz IG, Timson DJ and Pey AL (2016) Experimental and computational evidence on conformational fluctuations as a source of catalytic defects in genetic diseases. *RSC Adv* **6**, 58604.
- 32 Vankova P, Salido E, Timson DJ, Man P and Pey AL (2019) A dynamic core in human NQO1 controls the functional and stability effects of ligand binding and their communication across the enzyme dimer. *Biomolecules* **9**, 728.
- 33 Abraham MJ, Murtola T, Schulz R, Páli S, Smith JC, Hess B and Lindahl J (2015) GROMACS: High performance molecular simulations through multi-level parallelism from laptops to supercomputers. *SoftwareX* **1–2**, 19–25.
- 34 Humphrey W, Dalke A and Schulten K (1996) VMD: visual molecular dynamics. *J Mol Graph* **14**, 33–38, 27–8.
- 35 Lindorff-Larsen K, Piana S, Palmo K, Maragakis P, Klepeis JL, Dror RO and Shaw DE (2010) Improved side-chain torsion potentials for the Amber ff99SB protein force field. *Proteins* **78**, 1950–1958.
- 36 Wang J, Wolf RM, Caldwell JW, Kollman PA and Case DA (2004) Development and testing of a general amber force field. *J Comput Chem* **25**, 1157–1174.
- 37 Jorgensen WL, Chandrasekhar J, Madura JD, Impey RW and Klein ML (1983) Comparison of simple potential functions for simulating liquid water. *J Chem Phys* **79**, 926–935.
- 38 Rizzuti B, Bartucci R, Sportelli L and Guzzi R (2015) Fatty acid binding into the highest affinity site of human serum albumin observed in molecular dynamics simulation. *Arch Biochem Biophys* **579**, 18–25.
- 39 Evoli S, Mobley DL, Guzzi R and Rizzuti B (2016) Multiple binding modes of ibuprofen in human serum albumin identified by absolute binding free energy calculations. *Phys Chem Chem Phys* **18**, 32358–32368.
- 40 Loladze VV, Ibarra-Molero B, Sanchez-Ruiz JM and Makhatadze GI (1999) Engineering a thermostable protein via optimization of charge-charge interactions on the protein surface. *Biochemistry* **38**, 16419–16423.
- 41 Park C and Marqusee S (2004) Probing the high energy states in proteins by proteolysis. *J Mol Biol* **343**, 1467–1476.
- 42 Pey AL (2013) The interplay between protein stability and dynamics in conformational diseases: the case of hPGK1 deficiency. *Biochim Biophys Acta* **1834**, 2502–2511.
- 43 Asher G, Tsvetkov P, Kahana C and Shaul Y (2005) A mechanism of ubiquitin-independent proteasomal degradation of the tumor suppressors p53 and p73. *Genes Dev* **19**, 316–321.
- 44 Englander SW, Mayne L, Bay I and Sosnick TR (1997) Hydrogen exchange: the modern legacy of Lindstrom-Lang. *Protein Sci* **6**, 1101–1109.
- 45 Soskine M and Tawfik DS (2010) Mutational effects and the evolution of new protein functions. *Nat Rev Genet* **11**, 572–582.
- 46 Asher G, Dym O, Tsvetkov P, Adler J and Shaul Y (2006) The crystal structure of NAD(P)H quinone oxidoreductase 1 in complex with its potent inhibitor dicoumarol. *Biochemistry* **45**, 6372–6378.

Supporting information

Additional supporting information may be found online in the Supporting Information section at the end of the article.

Fig. S1. Hydrodynamic radii determined by DLS in hNQO1 samples.

Fig. S2. Native electrospray mass spectrometry of NQO1 protein variants.

Fig. S3. Proteolysis of NQO1_{holo} proteins by thermolysin.

Fig. S4. Interaction of NQO1 variants with SAMp73 as determined by NMR spectroscopy.

Fig. S5. Changes in HDX kinetics of hNQO1 due to the mutations H80R and S82D.

Fig. S6. HDX kinetics for protein segments (spanning residues 1–126) of hNQO1_{apo} variants for which at least one variant showed a value of $\Delta\%D_{av} > |10\%$ vs the WT protein.

Fig. S7. HDX kinetics for protein segments (spanning residues 127–271) of hNQO1_{apo} variants for which at least one variant showed a value of $\Delta\%D_{av} > |10\%$ vs the WT protein.

Fig. S8. HDX kinetics for protein segments of hNQO1_{holo} variants for which at least one variant showed a value of $\Delta\%D_{av} > |10\%$ vs the WT protein.

Fig. S9. Changes in electrostatic interactions derived from MD simulations.

Fig. S10. Effects of H80R and S82D mutation on the conformation (Δ RMSD) and dynamics (Δ RMSF) from MD simulations.

Appendix S1. Materials and methods